Advances in Applied Mathematics and Mechanics
Adv. Appl. Math. Mech., Vol. **10**, No. 2, pp. 424-444

DOI: 10.4208/aamm.OA-2016-0189
April 2018

Immersed Finite Element Method for Eigenvalue Problems in Elasticity

Seungwoo Lee[1], Do Young Kwak[1,*] and Imbo Sim[2]

[1] *Korea Advanced Institute of Science and Technology, Daehak Ro 291, Daejeon, Korea 34141*
[2] *National Institute for Mathematical Sciences 70, Yuseong-daero 1689, Daejeon, Korea 34047*

Received 17 November 2016, Accepted (in revised version) 25 July 2017

Abstract. We consider the approximation of eigenvalue problems for elasticity equations with interface. This kind of problems can be efficiently discretized by using immersed finite element method (IFEM) based on Crouzeix-Raviart P1-nonconforming element. The stability and the optimal convergence of IFEM for solving eigenvalue problems with interface are proved by adopting spectral analysis methods for the classical eigenvalue problem. Numerical experiments demonstrate our theoretical results.

AMS subject classifications: 65N30, 65N25

Key words: Immersed finite element, elasticity problem, eigenvalue.

1 Introduction

In this paper, we consider the approximation of eigenvalue problems with interface in elasticity. Eigenvalue analysis is an essential basis for many types of engineering analysis. As eigenvalues are closely related with the frequency and shape of structures, computing the eigensolutions is important to interpret the dynamic interaction between the structures. If the frequency of structures is close to the system's natural frequency, mechanical resonance occurs. It may lead to catastrophic failure or damage in constructed structures such as bridges, buildings, and towers [24]. In addition, eigenvalue analysis is applied to stability analysis for many physical problems such as thermoelastic problems [48] and fluid-solid interaction problems [5, 10, 20].

There have been mathematical studies of finite element methods for eigenvalue problems. We begin by pointing out the fundamental references [4, 21, 22, 43] for the analysis of eigenvalue problems. Babuška and Osborn provide the spectral analysis by using the

*Corresponding author.
Emails: woo528@kaist.ac.kr (S. Lee), kdy@kaist.ac.kr (D. Y. Kwak), imbosim@nims.re.kr (I. Sim)

properties of compact operators [4, 43]. The spectral approximation together with the case of general operators is presented in [21, 22]. In [46] various computed examples for Laplacian eigenproblems in planar regions are studied and there are references to physical problems where the results are relevant. For a nonconforming approximation of elliptic eigenvalue problems, it is shown that the eigenvalues computed by finite element methods give lower bounds of the exact eigenvalues whose eigenfunctions are singular in non-convex polygon [3]. The guaranteed lower and upper bounds of eigenvalues based on the nonconforming finite element approximation are given in [16]. Moreover, let us focus on eigenvalue problems in elasticity. A posteriori error estimator for linearized elasticity eigenvalue problems is studied in [47]. It is shown that upper and lower estimates for the error of eigenpairs are established in terms of a residual estimate and lower-order terms. In [42], a method for three-dimensional linear elasticity or shell problems is presented to derive computable estimates of the approximation error in eigenvalues. The spectral problem for the linear elasticity equations on curved non-convex domains, as well as with mixed boundary conditions is considered in [27]. Meddahi et al. [40] present an analysis for the eigenvalue problem of linear elasticity by means of a mixed variational formulation. This method weakly imposes the symmetry of the stress tensor and is free from the locking phenomenon.

When the elastic body is occupied by heterogeneous materials, it is known that governing equations contain the discontinuous material parameters along the interface of materials. To simulate such problems by finite element methods, a common strategy is to use fitted meshes along the interface. However, this strategy may require a very fine mesh near the interface. As an alternative approach, some numerical methods using unfitted meshes are proposed. One approach is an extended finite element method (XFEM) introduced by adding enrichment functions to the classical finite element space [23, 41]. Theoretical and computational results for XFEM in elasticity problems can be found in [7–9, 25, 32, 44].

Another method is an immersed finite element method (IFEM) [17,18,30,35,36] which can use any meshes independent of interface geometry. The idea of an IFEM is to construct local basis functions to satisfy the interface conditions without additional degrees of freedoms. For source problems with interface in elasticity, Kwak et al. [29] present a nonconforming IFEM based on the broken Crouzeix-Raviart (CR) element [19]. They prove optimal error estimates and provide numerical results for compressible and nearly incompressible materials. Computational results of IFEM based on the rotated Q_1-nonconforming element are reported in [37] and the related work in this direction can be found in [38]. In addition, the spectral analysis of IFEM for elliptic eigenvalue problems with an interface is given in [31]. Liu et al. [39] introduced a method which bears the same name *immersed finite element* to solve fluid solid interaction problem, but it is different from ours since they use double grids; one for solid another for fluid.

In this work, we analyze the spectral approximation of elasticity interface problems using P_1-nonconforming IFEM and derive the optimal convergence of eigenvalues. Moreover, we provide a series of numerical results of the eigenproblems with various

shapes of interface for compressible and incompressible materials. As a model problem, we consider an elasticity eigenvalue problem where the domain is separated into two subdomains by interface. The elastic modulus of the material is discontinuous along the interface and the eigenfunctions must satisfy certain interface conditions. We construct local basis functions to satisfy the jump conditions across the interface. Also our local basis functions are based on CR element. It is known that CR element does not lock on pure displacement problems [14]. For a traction boundary problem, the discrete scheme with a stabilization term is introduced to overcome locking [26]. Since interface conditions are related to traction conditions, IFEM based on CR elements does not suffer the effects of locking by adding the stabilization term. Furthermore, optimal orders of convergence for IFEM are proved in [29]. Exploiting the ideas of [29] we formulate the discrete scheme with the stabilization term. The proofs for the spectral correctness of IFEM are based on the analysis of [4, 21, 22, 43]. Introducing a solution operator, we use spectral properties of compact and self-adjoint operators in Banach space [1, 2, 6, 15]. In our analysis, we adopt the approximation properties of IFEM from [29] to establish the spectral analysis of IFEM. Our proofs for such spectral approximation are similar to the proofs of [31] which introduced IFEM to an elliptic eigenvalue problem with an interface.

The outline of this paper is as follows. In the next section, we give a description of elasticity eigenvalue problems with interface. In Section 3, we introduce a local basis function satisfying interface conditions and formulate an immersed finite element method with a stabilization term. Section 4 is devoted to the analysis of the spectral approximation which is proved to be spurious-free. In Section 5, we carry out numerical experiments for our model problem. The results demonstrate spurious-free and locking-free character of IFEM. Finally, we conclude the paper in Section 6.

2 Model problem

Let Ω be a connected and convex polygonal domain in $\mathbb{R}^2$ which is divided into two subdomains Ω^+ and Ω^- by a C^2 interface $\Gamma=\partial\Omega^+\cap\partial\Omega^-$ (see Fig. 1). We assume that the subdomains Ω^+ and Ω^- are occupied by two different elastic materials. Let λ and μ denote the Lamé coefficients given by

$$\lambda=\frac{E\nu}{(1+\nu)(1-2\nu)},\quad \mu=\frac{E}{2(1+\nu)},$$

where E is the Young's modulus and ν is the Poisson ratio. We note that the coefficients λ and μ are $0<\mu_1<\mu<\mu_2$ and $0<\lambda<\infty$. The constitutive equation is related to the displacement field $\mathbf{u}:=(u_i)\in\mathbb{R}^2$ and the Cauchy stress tensor $\boldsymbol{\sigma}:=(\sigma_{ij})\in\mathbb{R}^{2\times2}$ is given by

$$\boldsymbol{\sigma}(\mathbf{u})=2\mu\boldsymbol{\epsilon}(\mathbf{u})+\lambda tr(\boldsymbol{\epsilon}(\mathbf{u}))\boldsymbol{I},$$

where $\boldsymbol{I}$ is the identity matrix of $\mathbb{R}^{2\times2}$, the linearized strain tensor $\boldsymbol{\epsilon}:=(\epsilon_{ij})\in\mathbb{R}^{2\times2}$ is

$$\boldsymbol{\epsilon}(\mathbf{u})=\frac{1}{2}(\nabla\mathbf{u}+\nabla\mathbf{u}^T),$$

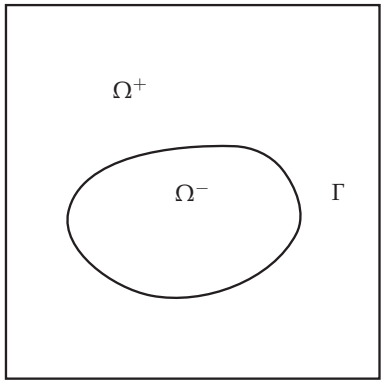

Figure 1: A domain Ω with interface.

and the usual trace operator $tr(\boldsymbol{\epsilon})$ is

$$tr(\boldsymbol{\epsilon}) := \sum_{i=1}^{2} \epsilon_{ii}.$$

For the sake of simplicity, we assume that the density $\rho > 0$ is a piecewise constant in subdomains Ω^+ and Ω^-. From now on, we consider the Lamé coefficients λ and μ as $\lambda := \lambda/\rho$ and $\mu := \mu/\rho$. Let us consider the eigenvalue problem for the linear elasticity equation with interface, i.e.,

$$-\operatorname{div}\boldsymbol{\sigma}(\mathbf{u}) = \omega^2 \mathbf{u} \quad \text{in } \Omega^s \quad (s = +,-), \tag{2.1a}$$
$$[\mathbf{u}]_\Gamma = 0, \tag{2.1b}$$
$$[\boldsymbol{\sigma}(\mathbf{u})\cdot\mathbf{n}]_\Gamma = 0, \tag{2.1c}$$
$$\mathbf{u} = 0 \quad \text{on } \partial\Omega, \tag{2.1d}$$

where ω^2 and $\mathbf{u}$ are the corresponding eigenvalue and eigenfunction, $\mathbf{n}$ is a unit normal vector of the interface Γ from Ω^- to Ω^+, and the symbol $[\cdot]$ denotes the jump across the interface Γ.

We formulate the model problem (2.1) into the displacement formulation [11]. Multiplying $\mathbf{v} \in (H_0^1(\Omega))^2$ and applying Green's identity to model problem (2.1) in each domain Ω^s, we obtain

$$\int_{\Omega^s} 2\mu\boldsymbol{\epsilon}(\mathbf{u}) : \boldsymbol{\epsilon}(\mathbf{v}) dx + \int_{\Omega^s} \lambda \operatorname{div}\mathbf{u} \operatorname{div}\mathbf{v} dx - \int_{\partial\Omega^s} \boldsymbol{\sigma}(\mathbf{u})\mathbf{n}\cdot\mathbf{v} ds = \omega^2 \int_{\Omega^s} \mathbf{u}\cdot\mathbf{v} dx,$$

where

$$\boldsymbol{\epsilon}(\mathbf{u}) : \boldsymbol{\epsilon}(\mathbf{v}) = \sum_{i,j=1}^{2} \epsilon_{ij}(\mathbf{u})\epsilon_{ij}(\mathbf{v}).$$

Summing over $s=+,-$ and applying the interface condition (2.1c), we have the following weak formulation

$$a(\mathbf{u},\mathbf{v})=\omega^2(\mathbf{u},\mathbf{v}), \tag{2.2}$$

where

$$a(\mathbf{u},\mathbf{v})=\int_\Omega 2\mu\boldsymbol{\epsilon}(\mathbf{u}):\boldsymbol{\epsilon}(\mathbf{v})dx+\int_\Omega \lambda \mathrm{div}\,\mathbf{u}\mathrm{div}\,\mathbf{v}dx$$

and

$$\omega^2(\mathbf{u},\mathbf{v})=\omega^2\int_\Omega \mathbf{u}\cdot\mathbf{v}dx.$$

3 Immersed finite element method

In this section, we introduce an immersed finite element method (IFEM) based on Crouzeix-Raviart elements [19]. Let $\{\mathcal{K}_h\}$ be usual quasi-uniform triangulations of the domain Ω by the triangles of maximum diameter h. Note that an element $K\in\mathcal{K}_h$ is not necessarily aligned with the interface Γ. For a smooth interface, provided that h is sufficiently small, we are able to assume that the interface intersects the edge of an element at no more than two points and joins each edge at most once, except possibly it passes through two vertices. According to [12, 13, 45], piecewise linear approximation of interface yields optimal convergence properties for the linear basis functions. Therefore, we may replace $\Gamma\cap K$ by the line segment joining two intersection points on the edges of each $K\in\mathcal{K}_h$. We call an element $K\in\mathcal{K}_h$ an *interface element* if the interface Γ passes through the interior of K, otherwise K is a *non-interface element*. Additionally we introduce some symbols:

- $\mathcal{K}_h^*$–the collection of all interface elements.
- $\mathcal{E}_h$–the collection of all the edges of $K\in\mathcal{K}_h$.

We construct local basis functions on each element K of the triangulation $\mathcal{K}_h$. For a non-interface element $K\in\mathcal{K}_h$, we choose a standard P_1-nonconforming basis whose degrees of freedom are determined by average values on each edge of an element K. Let $\mathbf{N}_h(K)$ denote the linear space spanned by the six Lagrange basis functions

$$\boldsymbol{\phi}_i=(\phi_{i1},\phi_{i2})^T,\quad i=1,2,\cdots,6,$$

satisfying

$$\frac{1}{|e_j|}\int_{e_j}\phi_{i1}ds=\delta_{ij},$$
$$\frac{1}{|e_j|}\int_{e_j}\phi_{i2}ds=\delta_{(i-3)j},$$

for each edge e_j of an element K, $j=1,2,3$. The P_1-nonconforming space $\mathbf{N}_h(\Omega)$ is given by

$$\mathbf{N}_h(\Omega)=\left\{\begin{array}{l}\boldsymbol{\phi}=(\phi_1,\phi_2)|_K\in\mathbf{N}_h(K) \text{ for each } K\in\mathcal{K}_h,\\ \text{if } K_1,K_2\in\mathcal{K}_h \text{ share an edge } e, \text{ then, for } i=1,2,\\ \int_e\phi_i|_{\partial K_1}ds=\int_e\phi_i|_{\partial K_2}ds \text{ and } \int_{\partial K\cap\partial\Omega}\phi_i ds=0.\end{array}\right\}$$

For an interface element $K\in\mathcal{K}_h^*$ (see Fig. 2), we describe how to construct the basis functions which satisfy the interface conditions (2.1b), (2.1c). The piecewise linear basis function $\widehat{\boldsymbol{\phi}}_i$, $i=1,2,\cdots,6$, of the form

$$\widehat{\boldsymbol{\phi}}_i(x,y)=\left\{\begin{array}{ll}\widehat{\boldsymbol{\phi}}_i^{+}(x,y)=\begin{pmatrix}\hat{\phi}_{i1}^{+}\\ \hat{\phi}_{i2}^{+}\end{pmatrix}=\begin{pmatrix}a_0^{+}+b_0^{+}x+c_0^{+}y\\ a_1^{+}+b_1^{+}x+c_1^{+}y\end{pmatrix}, & (x,y)\in K^{+},\\ \widehat{\boldsymbol{\phi}}_i^{-}(x,y)=\begin{pmatrix}\hat{\phi}_{i1}^{-}\\ \hat{\phi}_{i2}^{-}\end{pmatrix}=\begin{pmatrix}a_0^{-}+b_0^{-}x+c_0^{-}y\\ a_1^{-}+b_1^{-}x+c_1^{-}y\end{pmatrix}, & (x,y)\in K^{-},\end{array}\right.$$

satisfies

$$\frac{1}{|e_j|}\int_{e_j}\hat{\phi}_{i1}ds=\delta_{ij}, \qquad j=1,2,3, \tag{3.1a}$$

$$\frac{1}{|e_j|}\int_{e_j}\hat{\phi}_{i2}ds=\delta_{(i-3)j}, \qquad j=1,2,3, \tag{3.1b}$$

$$[\widehat{\boldsymbol{\phi}}_i(D)]=0, \tag{3.1c}$$

$$[\widehat{\boldsymbol{\phi}}_i(E)]=0, \tag{3.1d}$$

$$\left[\boldsymbol{\sigma}(\widehat{\boldsymbol{\phi}}_i)\cdot\mathbf{n}\right]_{\overline{DE}}=0. \tag{3.1e}$$

We can express these conditions as a square system of linear equations in twelve unknowns for each basis function $\widehat{\boldsymbol{\phi}}_i$. It is shown that this system has a unique solution regardless of the location of the interface (see [29]). Let us denote $\widehat{\mathbf{N}}_h(K)$ as the space of functions on an interface element K, which is generated by $\widehat{\boldsymbol{\phi}}_i$, $i=1,2,\cdots,6$. Using this local finite element space, we define the global *immersed finite element space* $\widehat{\mathbf{N}}_h(\Omega)$ by

$$\widehat{\mathbf{N}}_h(\Omega)=\left\{\begin{array}{l}\widehat{\boldsymbol{\phi}}\in\widehat{\mathbf{N}}_h(K) \text{ if } K\in\mathcal{K}_h^*, \text{ and } \widehat{\boldsymbol{\phi}}\in\mathbf{N}_h(K) \text{ if } K\notin\mathcal{K}_h^*,\\ \text{if } K_1 \text{ and } K_2 \text{ share an edge } e, \text{ then } \widehat{\boldsymbol{\phi}}=(\hat{\phi}_1,\hat{\phi}_2) \text{ satisfies},\\ \int_e\hat{\phi}_i|_{\partial K_1}ds=\int_e\hat{\phi}_i|_{\partial K_2}ds \text{ and } \int_{\partial K\cap\partial\Omega}\hat{\phi}_i ds=0, \quad (i=1,2).\end{array}\right\}$$

In order to describe the analysis of IFEM, we introduce some spaces and their norms. For a bounded domain D and non-negative integer m, we let $H^m(D)=W_2^m(D)$ be the usual Sobolev space of order m with norm (semi)-norms denoted by $\|\cdot\|_{m,D}$ ($|\cdot|_{m,D}$) and let

$$(\widetilde{H}^m(D))^2:=\{\mathbf{u}\in(H^{m-1}(D))^2:\mathbf{u}|_{D\cap\Omega^s}\in(H^m(D\cap\Omega^s))^2,\ s=+,-\},$$

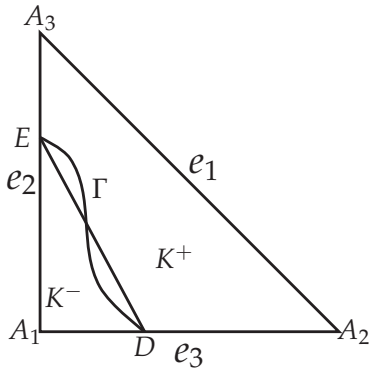

Figure 2: An interface triangle

equipped with norms

$$|\mathbf{u}|^2_{\widetilde{H}^m(D)} := |\mathbf{u}|^2_{m,D\cap\Omega^+} + |\mathbf{u}|^2_{m,D\cap\Omega^-},$$
$$\|\mathbf{u}\|^2_{\widetilde{H}^m(D)} := \|\mathbf{u}\|^2_{m,D\cap\Omega^+} + \|\mathbf{u}\|^2_{m,D\cap\Omega^-}.$$

In addition, we define the space $\mathbf{H}_h(\Omega)$ by $\mathbf{H}_h(\Omega) := (H^1_0(\Omega))^2 + \widehat{\mathbf{N}}_h(\Omega)$.

The IFEM for the eigenvalue problem (2.1) is to find the eigensolution $(\omega_h^2, \mathbf{u}_h) \in \mathbb{R} \times \widehat{\mathbf{N}}_h(\Omega)$ such that

$$a_h(\mathbf{u}_h, \mathbf{v}_h) = \omega_h^2(\mathbf{u}_h, \mathbf{v}_h), \qquad \forall \mathbf{v}_h \in \widehat{\mathbf{N}}_h(\Omega), \tag{3.2}$$

where

$$a_h(\mathbf{u},\mathbf{v}) := \sum_{K\in\mathcal{K}_h} \int_K 2\mu\boldsymbol{\epsilon}(\mathbf{u}) : \boldsymbol{\epsilon}(\mathbf{v}) dx + \sum_{K\in\mathcal{K}_h} \int_K \lambda \operatorname{div}\mathbf{u} \operatorname{div}\mathbf{v} dx$$
$$+ \sum_{e\in\mathcal{E}_h} \frac{\tau}{h} \int_e [\mathbf{u}][\mathbf{v}] ds, \quad \forall \mathbf{u},\mathbf{v} \in \mathbf{H}_h(\Omega). \tag{3.3}$$

The parameter τ in the bilinear form $a_h(\cdot,\cdot)$ is a positive constant which is independent of the mesh size h [26, 29]. We define the mesh dependent norm $\|\cdot\|_{a,h}$ on the space $\mathbf{H}_h(\Omega)$ by

$$\|\mathbf{v}\|^2_{a,h} := \sum_{K\in\mathcal{K}_h} \|\mathbf{v}\|^2_{a,K} + \sum_{e\in\mathcal{E}_h} \int_e \frac{\tau}{h} [\mathbf{v}]^2 ds,$$

where

$$\|\mathbf{v}\|^2_{a,K} = \int_K 2\mu\boldsymbol{\epsilon}(\mathbf{v}) : \boldsymbol{\epsilon}(\mathbf{v}) dx + \int_K \lambda |\operatorname{div}\mathbf{v}|^2 dx.$$

Remark 3.1. The idea of the discrete scheme is motivated from Hansbo and Larson [26]. For a source problem without an interface, they prove an optimal convergence of the scheme. For the problem with an interface, Kwak et al. [29] show the scheme yields an optimal result.

The coerciveness and boundedness of the bilinear form $a_h(\cdot,\cdot)$ are satisfied [29].

Theorem 3.1. *There exist positive constants C_b and C_c such that*

$$|a_h(\mathbf{u},\mathbf{v})| \le C_b\|\mathbf{u}\|_{a,h}\|\mathbf{v}\|_{a,h}, \qquad \forall \mathbf{u},\mathbf{v}\in\mathbf{H}_h(\Omega),$$
$$a_h(\mathbf{v},\mathbf{v}) \ge C_c\|\mathbf{v}\|_{a,h}^2, \qquad \forall \mathbf{v}\in\widehat{\mathbf{N}}_h(\Omega).$$

4 Spectral approximation

To analyze the spectral approximation, we introduce the solution operator $T:(L^2(\Omega))^2\to(H_0^1(\Omega))^2$, which associates the solution $T\mathbf{f}\in(H_0^1(\Omega))^2$ of the following source problem with every $\mathbf{f}\in(L^2(\Omega))^2$,

$$a(T\mathbf{f},\mathbf{v}) = (\mathbf{f},\mathbf{v}), \quad \forall \mathbf{v}\in(H_0^1(\Omega))^2.$$

The operator T is well-defined because unique solvability for every $\mathbf{f}\in(L^2(\Omega))^2$ is shown in [25,33]. Since it is clear that the operator T is self-adjoint and compact, the eigenvalues ξ of operator T belong to $\mathbb{R}$ [28]. In view of the definition of the solution operator T, if $(\omega^2,\mathbf{u})\in\mathbb{R}\setminus\{0\}\times(H_0^1(\Omega))^2$ is an eigenpair of the problem (2.2), then $(1/\omega^2,\mathbf{u})$ is an eigenpair for the operator T. In a similar way, we can define the corresponding discrete solution operator $T_h:(L^2(\Omega))^2\to\widehat{\mathbf{N}}_h(\Omega)$ by

$$a_h(T_h\mathbf{f},\mathbf{v}_h) = (\mathbf{f},\mathbf{v}_h), \quad \forall \mathbf{v}_h\in\widehat{\mathbf{N}}_h(\Omega),$$

with $\mathbf{f}\in(L^2(\Omega))^2$. Clearly, T_h is also a self-adjoint and compact operator. Notice that an eigenvalue ξ_h of the operator T_h is given by $\xi_h = 1/\omega_h^2$ where ω_h^2 is an eigenvalue of the discrete problem (3.2).

Before we show the uniform convergence of T_h to T, we state some assumptions which are suggested in [29] to analyze the IFEM for the source problem associated with the model problem (2.1).

- (H1). There exists a constant $C>0$ such that for $\mathbf{f}\in(L^2(\Omega))^2$,

$$2\mu\|T\mathbf{f}\|_{\widetilde{H}^2(\Omega)} + \lambda\|\mathrm{div}(T\mathbf{f})\|_{\widetilde{H}^1(\Omega)} \le C\|\mathbf{f}\|_{0,\Omega}.$$

- (H2). Given $\mathbf{f}\in(L^2(\Omega))^2$, it holds $\sigma(T\mathbf{f})\mathbf{n}\in(H^1(K))^2$ for each element $K\in\mathcal{K}_h$, where $\mathbf{n}$ is unit normal vector of K.

In fact, the hypothesis (H1) implies the regularity estimate which is known when the Lamé coefficients are continuous on the domain [26]. On the other hand, such estimate for the interface problems is not available to the best of authors' knowledge. The hypothesis (H2) is required to analyze the consistency error of the scheme (3.3). From now on, we assume the hypotheses (H1) and (H2).

The following theorem [29] states the uniform convergence of T_h to T which plays an important role in spectral approximation.

Theorem 4.1. *There exists a constant $C>0$ such that*

$$\|T\mathbf{f}-T_h\mathbf{f}\|_{0,\Omega}+h\|T\mathbf{f}-T_h\mathbf{f}\|_{a,h}\leq Ch^2\|\mathbf{f}\|_{0,\Omega},\quad \forall\mathbf{f}\in(L^2(\Omega))^2.$$

We are going to state the theoretical results of spectral approximation within the framework of [4, 21, 22]. Most proofs of theorems stated below are analogous to [31] which deals with the IFEM for elliptic eigenvalue problems. Let us introduce some notations for theoretical results. To state the convergence of operators, we introduce an operator norm $\|L\|_{\mathscr{L}(X,Y)}$ for a bounded linear operator $L:X\to Y$ by

$$\|L\|_{\mathscr{L}(X,Y)}=\sup_{x\in X}\frac{\|Lx\|_Y}{\|x\|_X}. \tag{4.1}$$

The distance between eigenspaces is evaluated by means of distance functions

$$\mathrm{dist}_h(x,Y)=\inf_{y\in Y}\|x-y\|_{a,h},\quad \mathrm{dist}_h(X,Y)=\sup_{x\in X,\ \|x\|_{a,h}=1}\mathrm{dist}_h(x,Y),$$

where X and Y are closed subspaces of $\mathbf{H}_h(\Omega)$. We denote by $\sigma(T)$ and $\rho(T)$ ($\sigma(T_h)$ and $\rho(T_h)$) the spectrum and resolvent set of the solution operator T (resp. T_h), respectively. For any $z\in\rho(T)$, the resolvent operator $R_z(T)$ is defined by $R_z(T)=(z-T)^{-1}$ from $(L^2(\Omega))^2$ to $(L^2(\Omega))^2$ or from $(H_0^1(\Omega))^2$ to $(H_0^1(\Omega))^2$ and the discrete resolvent operator $R_z(T_h)$ is defined by $R_z(T_h)=(z-T_h)^{-1}$ from $\mathbf{H}_h(\Omega)$ and $\mathbf{H}_h(\Omega)$ [28].

To show that the resolvent operators $R_z(T)$ and $R_z(T_h)$ are well-defined and bounded, we introduce the following theorem.

Theorem 4.2. *For $z\in\rho(T)$, $z\neq0$ and h small enough, there are constants $C_1,C_2>0$ depending on only Ω and $|z|$ such that*

$$\|(z-T)\mathbf{f}\|_{a,h}\geq C_1\|\mathbf{f}\|_{a,h},\qquad \forall\mathbf{f}\in\mathbf{H}_h(\Omega), \tag{4.2a}$$

$$\|(z-T_h)\mathbf{f}\|_{a,h}\geq C_2\|\mathbf{f}\|_{a,h},\qquad \forall\mathbf{f}\in\mathbf{H}_h(\Omega). \tag{4.2b}$$

Proof. The proof of the first inequality (4.2a) is essentially identical to that of Lemma 4.1 from [31]. The second inequality (4.2b) follows from the first inequality (4.2a) and Theorem 4.1 (see Lemma 1 in [21]). □

Let ξ be an eigenvalue of T with algebraic multiplicity n and Λ be a Jordan curve in $\mathbb{C}$ containing ξ, which lies in $\rho(T)$ and does not enclose any other points of $\sigma(T)$. We define the spectral projection $E(\xi)$ from $(L^2(\Omega))^2$ into $(H_0^1(\Omega))^2$ by

$$E(\xi)=\frac{1}{2\pi i}\int_\Lambda R_z(T)dz.$$

Owing to Theorem 4.2, we can define the discrete spectral projection $E_h(\xi)$ from $(L^2(\Omega))^2$ into $\mathbf{H}_h(\Omega)$ for h small enough by

$$E_h(\xi)=\frac{1}{2\pi i}\int_\Lambda R_z(T_h)dz.$$

We simply denote the projections $E(\xi)$ and $E_h(\xi)$ by E and E_h, respectively.

Theorem 4.3. *The discrete projection operator E_h converges uniformly to the projection operator E, i.e., it holds that*

$$\lim_{h\to 0}\|E-E_h\|_{\mathscr{L}((L^2(\Omega))^2,\mathbf{H}_h(\Omega))}=0.$$

Proof. We remark the residual identity

$$R_z(T)-R_z(T_h)=R_z(T_h)(T-T_h)R_z(T),$$

so that

$$\begin{aligned}&\|E-E_h\|_{\mathscr{L}((L^2(\Omega))^2,\mathbf{H}_h(\Omega))}\\ &\leq\|R_z(T_h)\|_{\mathscr{L}(\mathbf{H}_h(\Omega),\mathbf{H}_h(\Omega))}\|T-T_h\|_{\mathscr{L}((L^2(\Omega))^2,\mathbf{H}_h(\Omega))}\cdot\|R_z(T)\|_{\mathscr{L}((L^2(\Omega))^2,(L^2(\Omega))^2)}.\end{aligned}$$

By Theorem 4.2 and Fredholm alternative [28], the resolvent operators $R_z(T_h)$ and $R_z(T)$ are bounded for h small enough. In addition, the operator T_h converges to T uniformly by Theorem 4.1. Therefore, we conclude the proof. □

Finally, we can say that the discrete problem (3.2) is a spectrally correct approximation of the problem (2.2), provided that the following theorem holds [21]. For the proofs of following results, we refer to those of Theorems 1, 2, 3 and 6 from [21].

Theorem 4.4.

- *(Non-pollution of the spectrum) Let $A\subset\mathbb{R}$ be an open set containing $\sigma(T)$. Then for sufficiently small h, $\sigma(T_h)\subset A$.*
- *(Non-pollution of the eigenspace)*

$$\lim_{h\to 0}\mathrm{dist}_h(E_h(\mathbf{H}_h(\Omega)),E((H_0^1(\Omega))^2))=0.$$

- *(Completeness of the eigenspace)*

$$\lim_{h\to 0}\mathrm{dist}_h(E((H_0^1(\Omega))^2),E_h(\mathbf{H}_h(\Omega)))=0.$$

- *(Completeness of the spectrum) For all $z\in\sigma(T)$,*

$$\lim_{h\to 0}\mathrm{dist}_h(z,\sigma(T_h))=0.$$

It remains to show the convergence analysis of eigenvalues. The convergence rate of eigenvalues is obtained by the spectral properties of compact operators and the uniform convergence of the operator T_h to T in Theorem 4.1.

Theorem 4.5. *Let ξ be an eigenvalue of T with multiplicity n. Then for h small enough there exist n eigenvalues $\{\xi_{1,h},\cdots,\xi_{n,h}\}$ of T_h, which converge to ξ as follows*

$$\sup_{1\leq i\leq n}|\xi-\xi_{i,h}|\leq Ch^2,$$

where a positive constant C is independent of ξ and h.

Proof. The existence of eigenvalues $\xi_{i,h}$ is a direct consequence of Theorem 4.4. To estimate the convergence rate of $\xi_{i,h}$, we introduce some auxiliary operators. Let Φ_h and $\widetilde{T}$ be the restriction of operators E_h and T to $E((L^2(\Omega))^2)$, respectively. Following the arguments in [4, 43], we have that the inverse $\Phi_h^{-1}: E_h(\mathbf{H}_h(\Omega)) \to E((L^2(\Omega))^2)$ is bounded for h small enough. Hence we can define $\widetilde{T}_h := \Phi_h^{-1} T_h \Phi_h$ and $S_h := \Phi_h^{-1} E_h$. Note that the operator S_h is bounded and $S_h \mathbf{f} = \mathbf{f}$ for any $\mathbf{f} \in E((L^2(\Omega))^2)$. The auxiliary operators $\widetilde{T}$, $\widetilde{T}_h$, S_h and Φ_h provide a following property, for any $\mathbf{f} \in E((L^2(\Omega))^2)$,

$$\begin{aligned}(\widetilde{T}-\widetilde{T}_h)\mathbf{f} &= T\mathbf{f} - \Phi_h^{-1} T_h \Phi_h \mathbf{f} = S_h T\mathbf{f} - \Phi_h^{-1} T_h E_h \mathbf{f} \\ &= S_h T\mathbf{f} - \Phi_h^{-1} E_h T_h \mathbf{f} = S_h (T - T_h)\mathbf{f}.\end{aligned}$$

In view of definition of operator norm (4.1) and Theorem 4.1, we have

$$\begin{aligned}\sup_{1\le i\le n} |\xi - \xi_{i,h}| &\le C \|\widetilde{T} - \widetilde{T}_h\|_{\mathscr{L}(E((L^2(\Omega))^2), E((L^2(\Omega))^2))} \\ &= C \sup_{\mathbf{f}\in E((L^2(\Omega))^2)} \frac{\|(\widetilde{T}-\widetilde{T}_h)\mathbf{f}\|_{0,\Omega}}{\|\mathbf{f}\|_{0,\Omega}} \\ &= C \sup_{\mathbf{f}\in E((L^2(\Omega))^2)} \frac{\|S_h(T-T_h)\mathbf{f}\|_{0,\Omega}}{\|\mathbf{f}\|_{0,\Omega}} \\ &\le C \sup_{\mathbf{f}\in E((L^2(\Omega))^2)} \frac{\|(T-T_h)\mathbf{f}\|_{0,\Omega}}{\|\mathbf{f}\|_{0,\Omega}} \\ &\le C h^2.\end{aligned}$$

Thus, we complete the proof. □

Remark 4.1. Overall, we show that the IFEM is spurious-free and has optimal convergence property by Theorem 4.4 and Theorem 4.5. Although uniform convergence of solution operator which is essential basis for spectral analysis is based on the hypothesis (H1) and (H2), a variety of numerical results reported in the next section corroborate our theoretical results.

5 Numerical results

In this section we present a series of numerical experiments to verify the theoretical analysis for the approximation of the model problem (2.1) in the previous sections. We recall the definition of the Lamé coefficients of a material

$$\lambda = \frac{E\nu}{(1+\nu)(1-2\nu)}, \quad \mu = \frac{E}{2(1+\nu)},$$

where E is the Young's modulus and ν is the Poisson ratio. We carry out numerical tests for the cases of the compressible elastic materials ($\nu < 0.5$) and the nearly incompressible

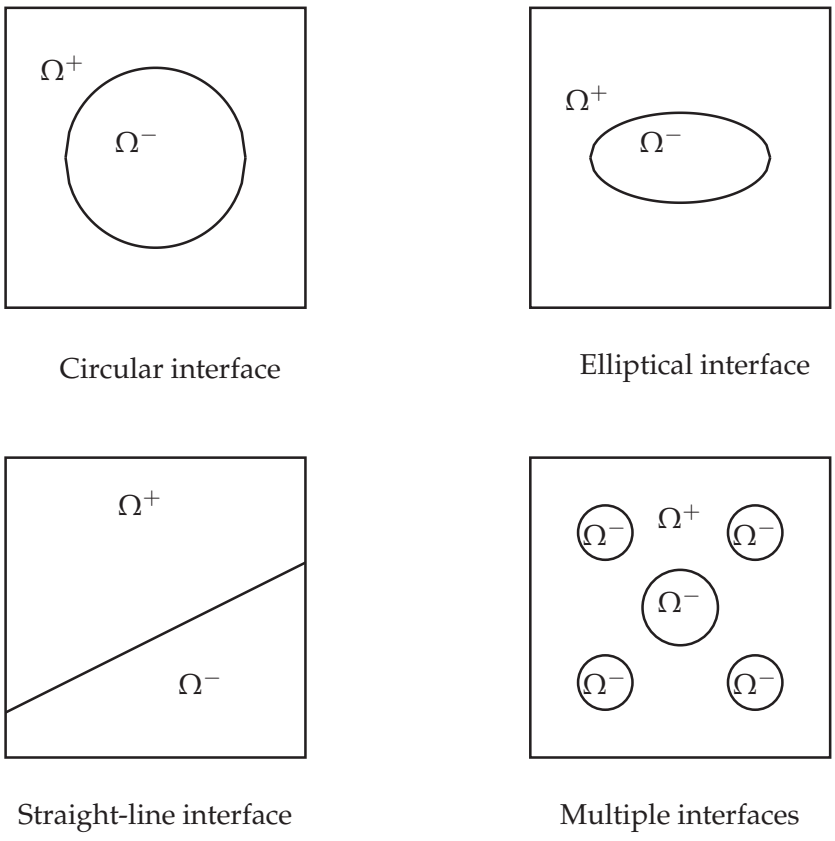

Figure 3: Domain and interfaces in Examples 5.1, 5.2, 5.3, 5.4 and 5.5.

elastic materials ($\nu \approx 0.5$) with various shapes of interface in Fig. 3. For a square domain $\Omega=[-1,1]^2$, we use uniform triangle meshes with mesh size $h=2/N$ where the refinement parameter N is the number of elements on each edge. Since analytical expressions for the eigenvalues are not available for all of the examples, we use the numerical results on a sufficiently refined mesh as the reference eigenvalues in order to estimate the order of convergence. In all the numerical examples, the IFEM is implemented in a C++ code and the eigenvalues are computed with ARPACK [34].

Example 5.1 (Circular interface)**.** In this example, we consider the eigenvalue problem (2.1) with a circular interface. The interface Γ is a circle with radius $r=0.6$ dividing $\Omega=[-1,1]^2$ into subdomains Ω^+ and Ω^- as follows,

$$\Omega^+ := \{(x,y) : x^2+y^2 > r^2\}, \quad \Omega^- := \{(x,y) : x^2+y^2 < r^2\}. \tag{5.1}$$

We set the Lamé coefficients as $(\mu^-,\mu^+) = (0.5,5),(5,0.5)$, $\lambda^\pm = 5\mu^\pm$ and Poisson ratio $\nu^\pm \approx 0.417$. Table 1 shows the first six eigenvalues ω_i^2, $i=1,2,\cdots,6$ in increasing order and

Table 1: First six eigenvalues computed by IFEM with circular interface for compressible materials. The reference eigenvalues ω^2_{ref} in the first column are computed with mesh size $h=1/2^9$. The numbers in parentheses show convergence rates.

Circular interface - $(\mu^-,\mu^+)=(0.5,5)$, $\lambda^\pm=5\mu^\pm$					
ω^2_{ref}	$h=1/2^3$	$h=1/2^4$(ord)	$h=1/2^5$(ord)	$h=1/2^6$(ord)	$h=1/2^7$(ord)
18.824	20.409	19.197 (2.09)	18.915 (2.03)	18.846 (2.02)	18.829 (2.07)
23.384	24.040	23.545 (2.03)	23.420 (2.16)	23.392 (2.19)	23.385 (2.51)
23.385	24.953	23.832 (1.81)	23.499 (1.97)	23.413 (2.02)	23.391 (2.12)
40.666	43.609	41.349 (2.10)	40.831 (2.05)	40.706 (2.03)	40.675 (2.09)
40.667	49.381	42.751 (2.06)	41.182 (2.01)	40.795 (2.01)	40.698 (2.07)
45.938	51.811	47.431 (1.98)	46.291 (2.08)	46.023 (2.05)	45.957 (2.14)
Circular interface - $(\mu^-,\mu^+)=(5,0.5)$, $\lambda^\pm=5\mu^\pm$					
ω^2_{ref}	$h=1/2^3$	$h=1/2^4$(ord)	$h=1/2^5$(ord)	$h=1/2^6$(ord)	$h=1/2^7$(ord)
7.151	7.356	7.205 (1.93)	7.1652 (2.00)	7.155 (2.00)	7.1524 (2.06)
10.121	10.165	10.135 (1.63)	10.124 (2.21)	10.121 (1.99)	10.121 (2.20)
10.121	10.313	10.177 (1.76)	10.135 (1.98)	10.124 (1.98)	10.121 (2.07)
24.205	25.696	24.585 (1.97)	24.292 (2.12)	24.224 (2.15)	24.208 (2.35)
24.205	26.708	24.863 (1.93)	24.368 (2.01)	24.245 (2.03)	24.214 (2.12)
32.257	34.569	32.937 (1.77)	32.439 (1.90)	32.303 (1.97)	32.268 (2.06)

their rates of convergence. The first columns contain the reference eigenvalues computed with the very fine mesh size $h=2^{-9}$ and the other columns contain the eigenvalues obtained with IFEM for varying h. We observe that the convergence rates of the eigenvalue are quadratic. An eigenfunction for eigenvalue ω^2_4, together with x-component and y-component of eigenfunction, are depicted in Fig. 4.

Example 5.2 (Elliptical interface)**.** The second example concerns an elliptical interface given by $\Gamma=\{(x,y):x^2/a^2+y^2/b^2=1\}$, where $a=0.6$ and $b=0.3$. We set subdomain Ω^- to be an interior and Ω^+ to be the other part of the domain Ω, i.e.,

$$\Omega^+:=\{(x,y):x^2/a^2+y^2/b^2>1\},\quad \Omega^-:=\{(x,y):x^2/a^2+y^2/b^2<1\}. \tag{5.2}$$

Let Lamé coefficients be $(\mu^-,\mu^+)=(0.5,5),(5,0.5)$ and $\lambda^\pm=5\mu^\pm$. In Fig. 5, we show the errors of the first four eigenvalues ω^2_i, $1\le i\le 4$ computed by IFEM and corresponding order of convergence. The reference solution is the numerical results on a refined mesh with mesh size $h=2^{-9}$. Even though the interface becomes shaper than the circular interface, the optimal convergence for eigenvalues is obtained. We display an eigenfunction of eigenvalue ω^2_3 in Fig. 6 which is analogous to Fig. 4.

Example 5.3 (Straight-line interface)**.** We let an interface be a straight line as $\Gamma=\{(x,y):y=0.5x-0.2\}$ and the subdomians Ω^+ and Ω^- be

$$\Omega^+:=\{(x,y):y>0.5x-0.2\},\quad \Omega^-:=\{(x,y):y<0.5x-0.2\}. \tag{5.3}$$

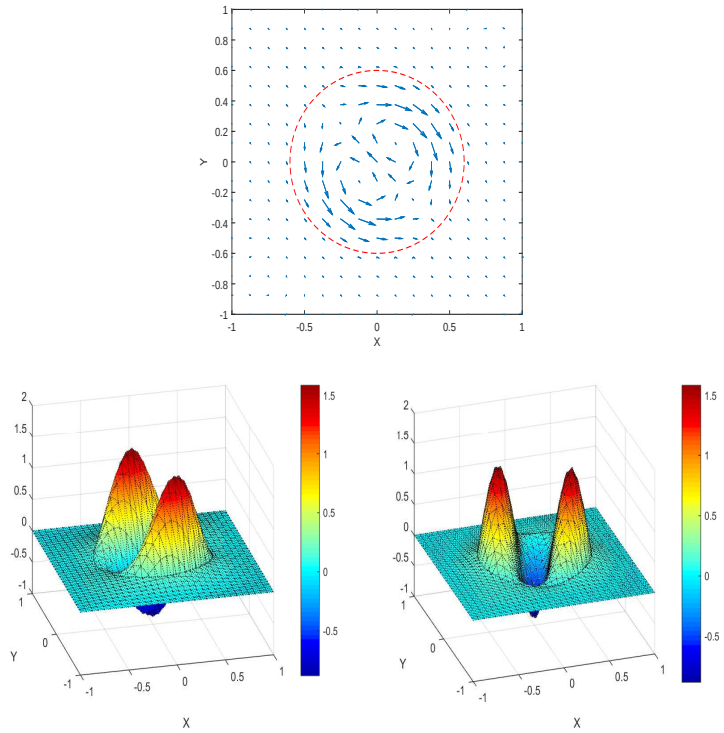

Figure 4: The figure above is an eigenfunction $\mathbf{u}$ of eigenvalue ω_4^2 when Lamé coefficients $(\mu^-,\mu^+)=(0.5,5)$, $\lambda^\pm=5\mu^\pm$ in Example 5.1. The figures below are x-component (left) and y-component (right) of eigenfunction $\mathbf{u}$ of eigenvalue ω_4^2.

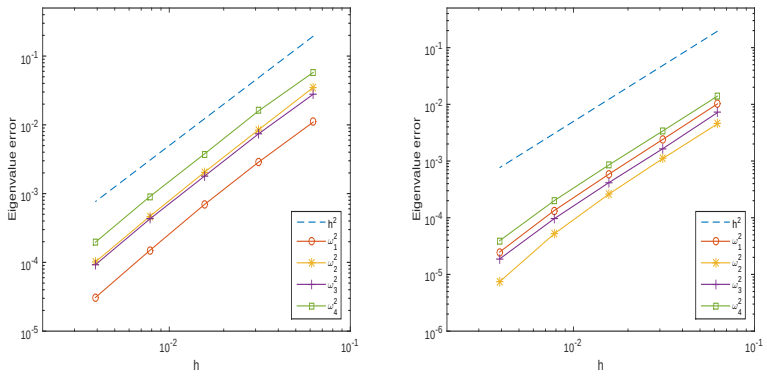

Figure 5: The log-log plots of mesh size h versus the relative error of the first four eigenvalues ω_1^2 (circle), ω_2^2 (asterisk), ω_3^2 (plus sign) and ω_4^2 (square) with an elliptical interface for the cases of Lamé coefficients $(\mu^-,\mu^+)=(0.5,5)$, $\lambda^\pm=\mu^\pm$ (left) and $(\mu^-,\mu^+)=(5,0.5)$, $\lambda^\pm=\mu^\pm$ (right) in Example 5.2. The broken line represents the optimal convergence rate.

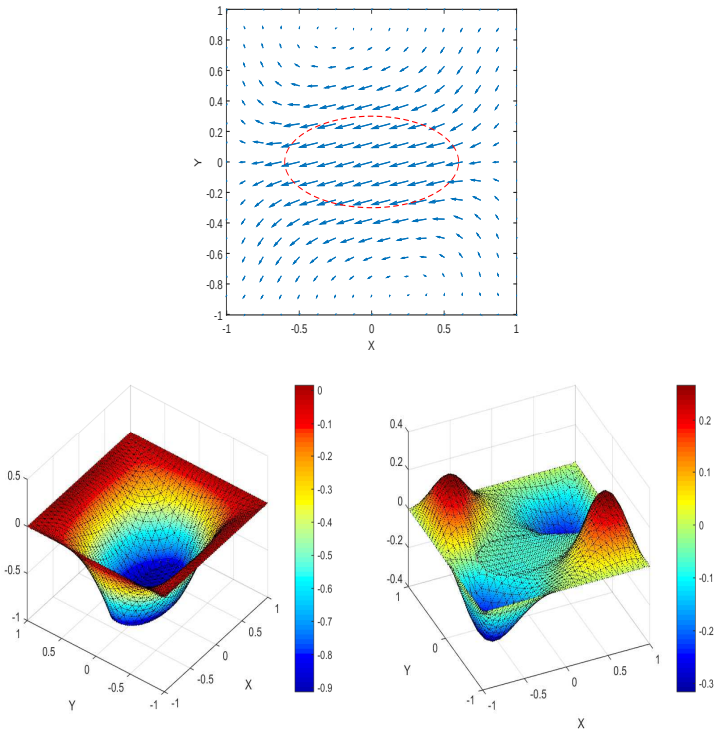

Figure 6: The figure above is an eigenfunction $\mathbf{u}$ of eigenvalue ω_3^2 for the case of an elliptical interface when Lamé coefficients $\mu^-=5$, $\mu^+=0.5$, $\lambda^\pm=5\mu^\pm$ in Example 5.2. The figures below are x-component of eigenfunction $\mathbf{u}$ on the left and y-component of eigenfunction $\mathbf{u}$ on the right.

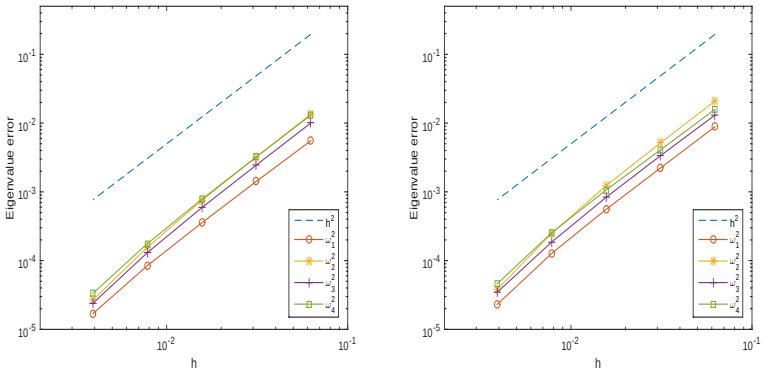

Figure 7: The log-log plots of mesh size h versus the relative error of the first four eigenvalues ω_1^2 (circle), ω_2^2 (asterisk), ω_3^2 (plus sign) and ω_4^2 (square) with a straight-line interface for the cases of Lamé coefficients $(\mu^-,\mu^+)=(0.5,5)$, $\lambda^\pm=\mu^\pm$ (left) and $(\mu^-,\mu^+)=(5,0.5)$, $\lambda^\pm=\mu^\pm$ (right) in Example 5.3. The broken line represents the optimal convergence rate.

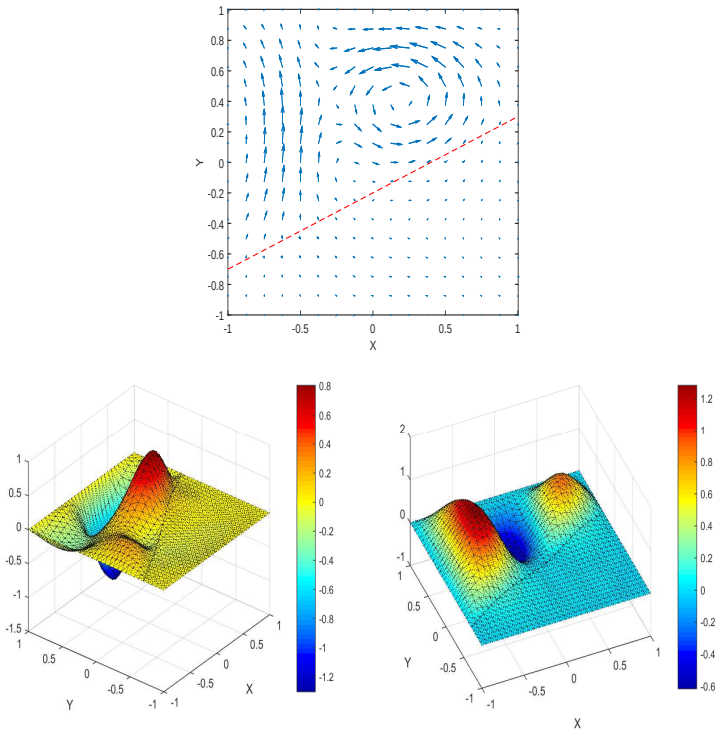

Figure 8: Eigenfunction $\mathbf{u}$ of eigenvalue ω_4^2 when Lamé coefficients $(\mu^-,\mu^+)=(0.5,5)$, $\lambda^\pm=5\mu^\pm$ in Example 5.3; eigenfunction $\mathbf{u}$ (above), x-component of eigenfunction $\mathbf{u}$ (below on the left), and y-component of eigenfunction $\mathbf{u}$ (below on the right).

The Lamé coefficients are the same as previous examples, $(\mu^-,\mu^+)=(0.5,5),(5,0.5)$ and $\lambda^\pm=5\mu^\pm$. In Fig. 7, we show the errors of the first four eigenvalues ω_i^2, $1\leq i\leq 4$ computed with IFEM. This figure also presents that the rates of convergence are quadratic. Note that in this example the interface meets the boundary of the domain. Nevertheless, the order of convergence is optimal. Fig. 8 shows the computed eigenfunction corresponding to eigenvalue ω_4^2.

Example 5.4 (Multiple interfaces)**.** In this case, we solved the problem (2.1) with 5 circular interfaces. Let subdomains Ω^- and Ω^+ be as follows

$$\Omega^- = \cup_{i=1}^5 \{(x,y):(x-a_i)^2+(y-b_i)^2<r_i\},$$
$$\Omega^+ = \Omega\setminus\Omega^-,$$

where $(a_1,b_1)=(0,0)$, $r_1=0.26$ and $(a_i,b_i)=(\pm 0.5,\pm 0.5)$, $r_i=0.19$ for $2\leq i\leq 5$ (see Fig. 3). The Lamé coefficients are chosen as $(\mu^-,\lambda^-,\nu^-)=(1,2,0.33)$, $(\mu^+,\lambda^+,\nu^+)=(30,36,0.27)$. Fig. 9 illustrates the error and the rates of convergence for eigenvalues ω_i^2, $(1\leq i\leq 4)$ calculated by IFEM. The results in Fig. 9 are in good agreement with our theoretical analysis in the previous section. Fig. 10 depicts an eigenfunction of eigenvalue ω_7^2.

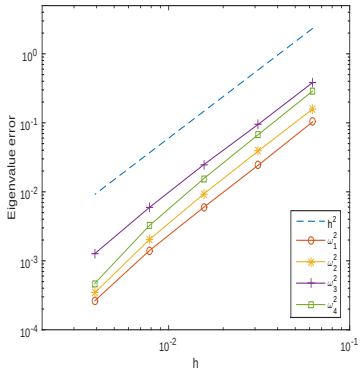

Figure 9: The log-log plot of mesh size h versus the relative error of the first four eigenvalues ω_1^2 (circle), ω_2^2 (asterisk), ω_3^2 (plus sign) and ω_4^2 (square) with multiple interfaces for the case of Lamé coefficients $(\mu^-,\lambda^-)=(1,2)$, $(\mu^+,\lambda^+)=(30,36)$ in Example 5.4. The broken line represents the optimal convergence rate.

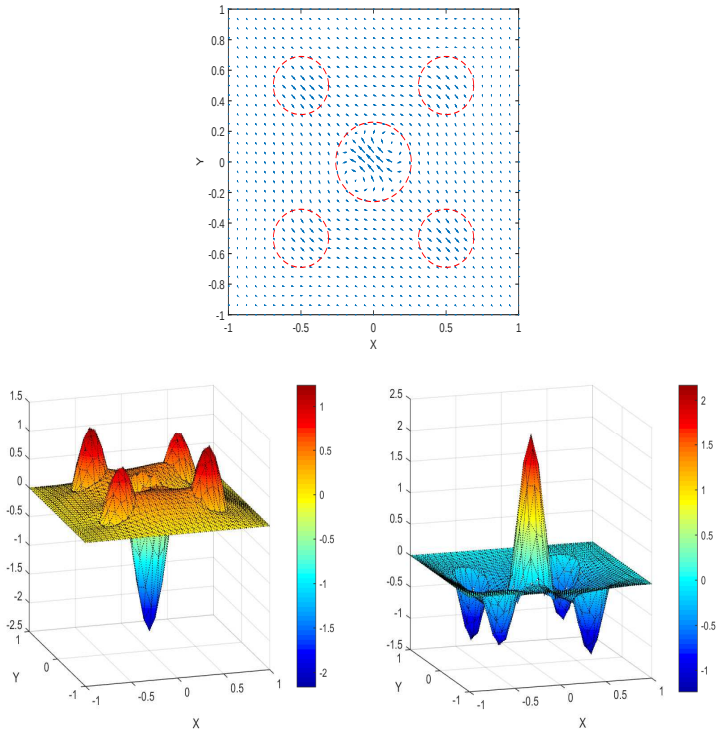

Figure 10: Eigenfunction $\mathbf{u}$ of eigenvalue ω_7^2 when Lamé coefficients $(\mu^-,\lambda^-)=(1,2)$, $(\mu^+,\lambda^+)=(30,36)$ in Example 5.4; eigenfunction $\mathbf{u}$ (above), x-component of eigenfunction $\mathbf{u}$ (below on the left), and y-component of eigenfunction $\mathbf{u}$ (below on the right).

Example 5.5 (Incompressible materials)**.** To experiment the case of the incompressible elastic materials, we set Lamé coefficients $(\mu^-,\mu^+)=(0.5,5),(5,0.5)$, $\lambda^\pm=5000\mu^\pm$ and $\nu^\pm\approx 0.4999$. We carry out similar numerical experiments with a straight-line interface to demonstrate the locking-free character of our method. The domain Ω and interface Γ are the same as Example 5.3. In Fig. 11, we report the errors of first four eigenvalues ω_i^2, $(1\le i\le 4)$ computed by IFEM. According to Fig. 11, we obtain that the method has thoroughly locking-free feature for solving the elasticity interface problems.

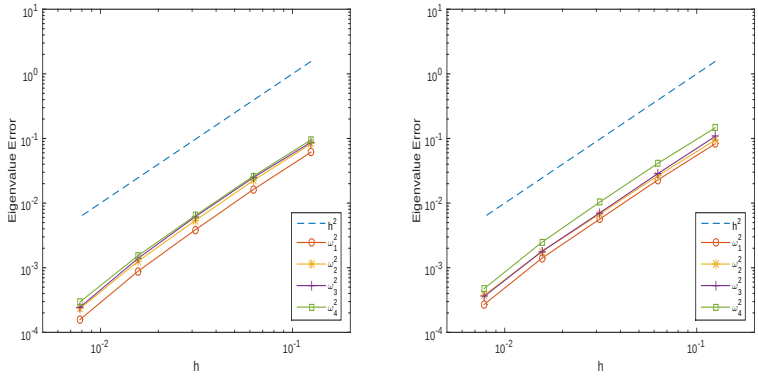

Figure 11: The log-log plots of mesh size h versus the relative error of the first four eigenvalues ω_1^2 (circle), ω_2^2 (asterisk), ω_3^2 (plus sign) and ω_4^2 (square) with incompressible materials ($\nu\approx 0.4999$) for the cases of $(\mu^-,\mu^+)=(0.5,5)$, $\lambda^\pm=\mu^\pm$ (left) and $(\mu^-,\mu^+)=(5,0.5)$, $\lambda^\pm=\mu^\pm$ (right) in Example 5.5. The broken line represents the optimal convergence rate.

6 Conclusions

This paper presents the IFEM for eigenvalue problems with interface in elasticity. The IFEM is based on Crouzeix-Raviart element with the stabilization term to circumvent locking phenomena. We show the spectral correctness and optimal convergence properties of the method within the framework of spectral analysis for a compact operator. Numerical results with various shapes of interfaces demonstrate the second-order convergence for eigenvalues. We also observe that the method is spurious-free and locking-free in all tests.

Acknowledgements

The authors are supported by grants from the National Research Foundation of Korea (NRF, No. 2017R1D1A1B03032765).

References

[1] A. Alonso and A. Dello Russo, *Spectral approximation of variationally-posed eigenvalue problems by nonconforming methods*, J. Comput. Appl. Math., 223 (2009), pp. 177–197.

[2] P. F. Antonietti, A. Buffa and I. Perugia, *Discontinuous Galerkin approximation of the Laplace eigenproblem*, Comput. Methods Appl. Mech. Eng., 195 (2006), pp. 3483–3503.

[3] M. G. Armentano and R. G. Durán, *Asymptotic lower bounds for eigenvalues by nonconforming finite element methods*, Electron. Trans. Numer. Anal., 17 (2004), pp. 93–101.

[4] I. Babuška and J. E. Osborn, Eigenvalue Problems, Handbook of Numerical Analysis II, North-Holland, Amsterdam, 1991.

[5] M. A. Barrientos, G. N. Gatica, R. Rodríguez and M. E. Torrejón, *Analysis of a coupled BEM/FEM eigensolver for the hydroelastic vibrations problem*, M2AN Math. Model. Numer. Anal., 38 (2004), pp. 653–672.

[6] C. Beattie, *Galerkin eigenvector approximations*, Math. Comput., 69 (2000), pp. 1409–1434.

[7] R. Becker, E. Burman and P. Hansbo, *A Nitsche extended finite element method for incompressible elasticity with discontinuous modulus of elasticity*, Comput. Methods Appl. Mech. Eng., 198 (2009), pp. 3352–3360.

[8] T. Belytschko and T. Black, *Elastic crack growth in finite elements with minimal remeshing*, Internat. J. Numer. Methods Eng., 45 (1999), pp. 601–620.

[9] T. Belytschko, C. Parimi, N. Moës, N. Sukumar and S. Usui, *Structured extended finite element methods for solids defined by implicit surfaces*, Int. J. Numer. Methods Eng., 56 (2003), pp. 609–635.

[10] A. Bermúdez, R. Durán and R. Rodríguez, *Finite element analysis of compressible and incompressible fluid-solid systems*, Math. Comput., 67 (1998), pp. 111–136.

[11] D. Braess, Finite Elements, Theory, Fast Solvers, and Applications in Solid Mechanics, 2nd ed., Cambridge University Press, Cambridge, 2001.

[12] J. H. Bramble and J. T. King, *A robust finite element method for nonhomogeneous Dirichlet problems in domains with curved boundaries*, Math. Comput., 63 (1994), pp. 1–17.

[13] J. H. Bramble and J. T. King, *A finite element method for interface problems in domains with smooth boundaries and interfaces*, Adv. Comput. Math., 6 (1996), pp. 109–138.

[14] S. C. Brenner and L. Y. Sung, *Linear finite element methods for planar linear elasticity*, Math. Comput., 59 (1992), pp. 321–338.

[15] A. Buffa and I. Perugia, *Discontinuous Galerkin approximation of the Maxwell eigenproblem*, SIAM J. Numer. Anal., 44 (2006), pp. 2198–2226.

[16] C. Carstensen and J. Gedicke, *Guaranteed lower bounds for eigenvalues*, Math. Comput., 83 (2014), pp. 2605–2629.

[17] K. S. Chang and D. Y. Kwak, *Discontinuous bubble scheme for elliptic problems with jumps in the solution*, Comput. Methods Appl. Mech. Eng., 200 (2011), pp. 494–508.

[18] S. H. Chou, D. Y. Kwak and K. T. Wee, *Optimal convergence analysis of an immersed interface finite element method*, Adv. Comput. Math., 33 (2010), pp. 149–168.

[19] M. Crouzeix and P. A. Raviart, *Conforming and nonconforming finite element methods for solving the stationary Stokes equations I*, Rev. Fr. Autom. Inf. Rech. Oper., 7 (1973), pp. 33–75.

[20] A. Dello Russo and A. Alonso, *Hybrid finite element analysis of fluid-structure systems with coupling on curved interfaces*, IMA J. Numer. Anal., 31 (2011), pp. 1636–1682.

[21] J. Descloux, N. Nassif and J. Rappaz, *On spectral approximation I. The problem of convergence*, RAIRO Anal. Numér., 12 (1978), pp. 97–112.

[22] J. Descloux, N. Nassif and J. Rappaz, *On spectral approximation II. Error estimates for the*

Galerkin method, RAIRO Anal. Numér., 12 (1978), pp. 113–119.
[23] T. P. FRIES AND T. BELYTSCHKO, *The extended/generalized finite element method: An overview of the method and its applications*, Int. J. Numer. Methods Eng., 84 (2010), pp. 253–304.
[24] D. GREEN AND W. G. UNRUH, *The failure of the Tacoma bridge: a physical model*, Amer. J. Phys., 74 (2006), pp. 706–716.
[25] A. HANSBO AND P. HANSBO, *A finite element method for the simulation of strong and weak discontinuities in solid mechanics*, Comput. Methods Appl. Mech. Eng., 193 (2004), pp. 3523–3540.
[26] P. HANSBO AND M. G. LARSON, *Discontinuous Galerkin and the Crouzeix-Raviart element: applications to elasticity*, M2AN Math. Model. Numer. Anal., 37 (2003), pp. 63–72.
[27] E. HERNÁNDEZ, *Finite element approximation of the elasticity spectral problem on curved domains*, J. Comput. Appl. Math., 225 (2009), pp. 452–458.
[28] T. KATO, Perturbation Theory for Linear Operators, Classics in Mathematics, Springer-Verlag, Berlin, 1995.
[29] D. Y. KWAK, S. JIN AND D. H. KYEONG, *A stabilized P_1 immersed finite element method for the interface elasticity problems*, to appear in ESAIM.
[30] D. Y. KWAK, K. T. WEE AND K. S. CHANG, *An analysis of a broken P_1-nonconforming finite element method for interface problems*, SIAM J. Numer. Anal., 48 (2010), pp. 2117–2134.
[31] S. LEE, D. Y. KWAK AND I. SIM, *Immersed finite element method for eigenvalue problem*, To appear in J. Comput. Appl. Math..
[32] G. LEGRAIN, N. MOËS AND E. VERRON, *Stress analysis around crack tips in finite strain problems using the extended finite element method*, Int. J. Numer. Methods Eng., 63 (2005), pp. 290–314.
[33] D. LEGUILLON AND E. SÁNCHEZ-PALENCIA, Computation of Singular Solutions in Elliptic Problems and Elasticity, John Wiley & Sons, Ltd., Chichester, Masson, Paris, 1987.
[34] R. B. LEHOUCQ, D. C. SORENSEN AND C. YANG, ARPACK Users' Guide: Solution of Large-Scale Eigenvalue Problems with Implicitly Restarted Arnoldi Methods, SIAM, Philadelphia, 1998.
[35] Z. LI, T. LIN, Y. LIN AND R. C. ROGERS, *An immersed finite element space and its approximation capability*, Numer. Methods Partial Differential Equations, 20 (2004), pp. 338–367.
[36] Z. LI, T. LIN AND X. WU, *New Cartesian grid methods for interface problems using the finite element formulation*, Numer. Math., 96 (2003), pp. 61–98.
[37] T. LIN, D. SHEEN AND X. ZHANG, *A locking-free immersed finite element method for planar elasticity interface problems*, J. Comput. Phys., 247 (2013), pp. 228–247.
[38] T. LIN AND X. ZHANG, *Linear and bilinear immersed finite elements for planar elasticity interface problems*, J. Comput. Appl. Math., 236 (2012), pp. 4681–4699.
[39] WING KAM LIU, DO WAN KIM AND SHAOQIANG TANG, *Mathematical foundations of the immersed finite element method*, Comput. Mech., 39 (2007), pp. 211–222.
[40] S. MEDDAHI, D. MORA AND R. RODRÍGUEZ, *Finite element spectral analysis for the mixed formulation of the elasticity equations*, SIAM J. Numer. Anal., 51 (2013), pp. 1041–1063.
[41] N. MOËS, J. DOLBOW AND T. BELYTSCHKO, *A finite element method for crack growth without remeshing*, Internat. J. Numer. Methods Eng., 46 (1999), pp. 131–150.
[42] J. T. ODEN, S. PRUDHOMME, T. WESTERMANN, J. BASS AND M. E. BOTKIN, *Error estimation of eigenfrequencies for elasticity and shell problems*, Math. Models Methods Appl. Sci., 13 (2003), pp. 323–344.
[43] J. E. OSBORN, *Spectral approximation for compact operators*, Math. Comput., 29 (1975), pp. 712–725.

[44] I. V. SINGH, B. K. MISHRA, S. BHATTACHARYA AND R. U. PATIL, *The numerical simulation of fatigue crack growth using extended finite element method*, Int J. Fatigue, 36 (2012), pp. 109–119.
[45] G. STRANG AND G. FIX, An Analysis of the Finite Element Method, 2nd ed., Wellesley-Cambridge Press, Wellesley, MA, 2008.
[46] L. N. TREFETHEN AND T. BETCKE, *Computed eigenmodes of planar regions*, Contemp. Math., 412 (2006), pp. 297–314.
[47] T. F. WALSH, G. M. REESE AND U. L. HETMANIUK, *Explicit a posteriori error estimates for eigenvalue analysis of heterogeneous elastic structures*, Comput. Methods Appl. Mech. Eng., 196 (2007), pp. 3614–3623.
[48] Y.-B. YI AND M. A. MATIN, *Eigenvalue solution of thermoelastic damping in beam resonators using a finite element analysis*, J. Vib. Acoust., 129 (2007), pp. 478–483.